Influence of micro-shrinkage on the fatigue behavior of ductile iron

Paul Kainzinger[1,*], Christoph Guster[1], Martin Severing[2], Anton Wolf[3]

[1] Chair of Mechanical Engineering, Montanuniversitaet Leoben, Leoben, Austria
[2] SHW Casting Technologies, Aalen-Wasseralfingen, Germany
[3] AMSC Austria, Klagenfurt, Austria
* Corresponding author: paul.kainzinger@unileoben.ac.at

Abstract Fatigue crack growth and conventional fatigue tests have been carried out from different sampling locations within a wind turbine hub. S/N curves as well as fatigue crack propagation properties have been determined in dependency of the local microstructure. Subsequent fractographic analysis of the conventional fatigue tests showed micro-shrinkage to be the dominant reason for crack initiation. Statistical analysis of these micro-shrinkages showed a relationship between their size and the local solidification conditions. A model is proposed, linking the size of the shrinkages and the fatigue strength of nodular cast iron. Using this model, it is possible to describe the fatigue strength of nodular cast iron in dependence of the local solidification conditions or local microstructure, respectively.

Keywords Ductile Iron, fatigue, defects, micro-shrinkage

1. Introduction

Nodular cast iron is widely used for structural components of wind turbines due to its very good castability. Guidelines and codes dominate the design process of such components, which are rather conservative regarding the tolerable stresses [1,2]. Although these components can easily weigh up to several ten tons, their material properties are far from homogeneous. Large wall thicknesses and added chill irons result in different solidification conditions leading to different microstructures. Different material properties arise, depending on the local microstructure. Casting simulation tools are able to estimate local solidification conditions and the resulting local static material properties [3]. If the materials full potential should be used, the estimation of the dynamic material properties using empirical relationships between static and dynamic properties, which is common for guidelines, is not sufficiently accurate. In this paper, the Kitagawa Takahashi diagram [4] modified by El-Haddad [5] is used to describe the local cyclic material properties of nodular cast iron based on metallographic parameters. Therefore, fatigue crack growth experiments as well as conventional fatigue tests have been carried out using specimen with different characteristic microstructures. The Woehler experiments used for these investigations have already been published in [6]. The results of further investigations of the fractured specimen's surfaces, as well as the results of crack growth experiments are presented in this paper.

2. Experimental Procedure

A wind turbine hub made of EN-GJS-400-18U-LT standardized in [7] was used as base material for these investigations. The material has been taken from different sampling locations within the wind turbine hub in order to retrieve material with various solidification conditions and microstructures resulting in different material properties. The reader is referred to [6] for a detailed description of the sampling locations.
Fatigue crack growth experiments have been carried out according to [8] at room temperature and ambient air using the direct current potential drop method. The specimens have been subjected to four-point bending loads. For further information on the testing equipment refer to [9].

Single edge notched specimens have been used, their geometry is illustrated in Figure 1. To ensure a sound specimen surface, all the specimens have been grinded using a P320 sandpaper. The notch of the specimens has been pre-scratched.
Crack growth tests have been carried out using R-ratios of R=-1, R=0 und R=0.3. Only the threshold of the stress intensity factor K_{th} has been evaluated.

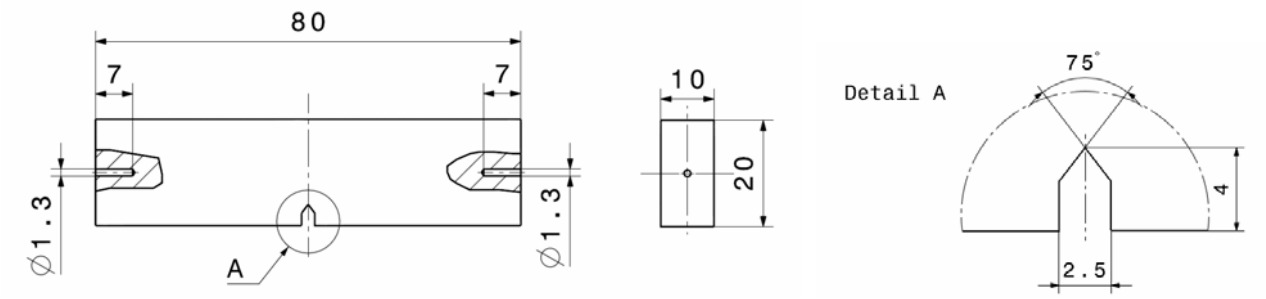

Figure 1: Geometry of the crack growth specimen

Constant amplitude Woehler experiments have been carried out at room temperature and ambient air. A resonance test rig Sincotec Exciting MAG was used to test the specimens up to 10^7 load cycles with a frequency of about 120Hz. All specimens have been tested under fully reversed loading (R=-1).
The finite life region was evaluated according to ASTM E739 [10]. The existence of a distinct fatigue limit is assumed according to [11], because the investigated material was fully ferritic and no retained austenite was found. The evaluation of the fatigue limit was carried out using the arcsin $\sqrt{p}$ transformation [12] with the estimator according to [13, 14].
Fractographic analysis of the fractured specimen surface has been carried out using a scanning electron microscope (Zeiss EVO MA15). Micro-shrinkages found in the fractured surfaces have been manually traced and two parameters (square root of particle area and maximum dimension) have been evaluated.

3. Crack Growth Experiments

At first, the specimens have been categorized using a qualitative measurement of the solidification rate depending on their sampling location (fast, medium, normal, slow). The number of tested specimen is available in Table 1.

Table 1: Test plan for the crack growth tests

Solidification speed	fast	medium	normal	slow	medium	slow	fast	medium	Slow
Stress-ratio R	0	0	0	0	0.3	0.3	-1	-1	-1
Number of samples	2	1	2	4	2	2	2	2	2

The results of the fatigue crack growth experiments are summarized in Figure 2. It is clearly visible, that the threshold K_{th} is decreasing with increasing stress ratio. Furthermore, the dependence of the microstructure becomes obvious, faster solidification (fine microstructure) leads to a lower threshold then slow solidification (coarse microstructure). The same trend has also been observed by Huebner et al. in [15] as well as Komber in [16] who also observed this trend for lamellar cast iron. She proposed a model to describe the threshold for crack initiation in dependence of microstructural parameters, namely the shape factor of the graphite nodules f and the mean distance between the graphite particles λ. This trend is contributed to the fact that the graphite particles act as crack stoppers. Huebner also observed lower crack growth rates in region II and a delayed transition to the region III for slower solidification rates in [15].

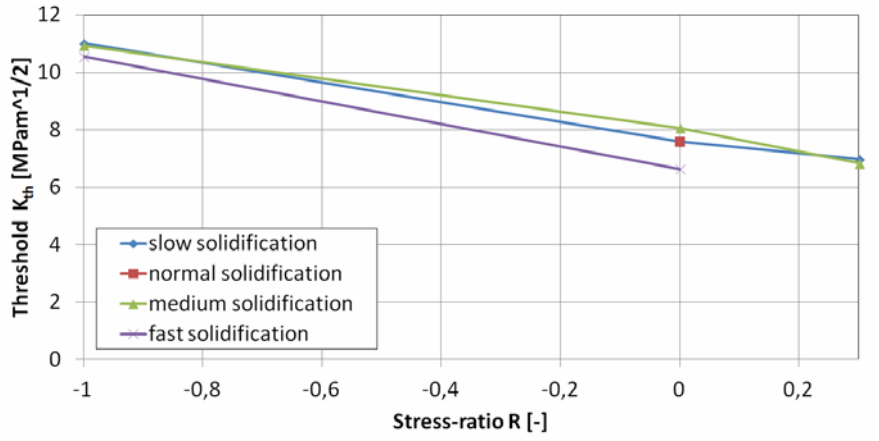

Figure 2: Threshold for crack propagation K_{th} in dependence of stress ratio and microstructure

To further quantify the solidification speed and to compare the results with those found in the literature, several metallographic parameters have been evaluated for each tested specimen. Therefore, the following parameters of the graphite particles from metallographic grindings made from each tested specimen have been evaluated:

- mean distance between the particles λ
- particle diameter d
- shape factor of the particle f
- number of particles per square millimeter n

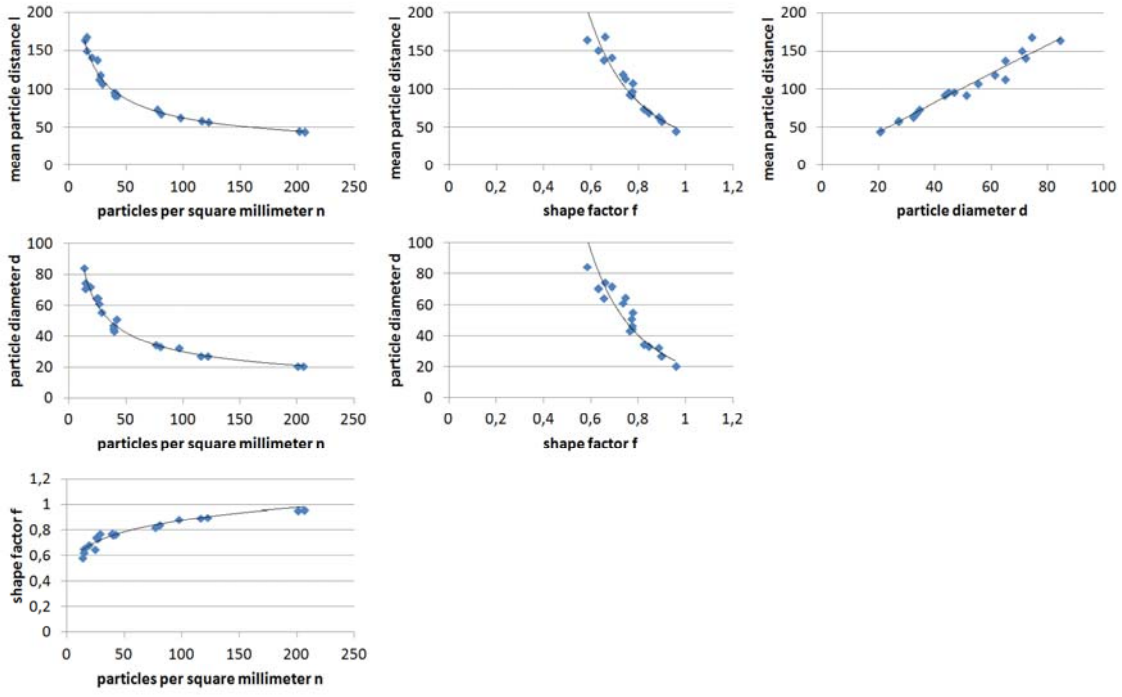

Figure 3: Comparison of the evaluated metallographic parameters (λ, d, f, n)

These four parameters have been plotted against each other in Figure 3. One can observe that all parameters are depending on each other. Slower solidification leads to larger mean distances λ, larger particle diameters d, smaller shape factors f (more degenerated graphite particles), a smaller number of particles n and vice verca. No distinct effect of the shape of the graphite nodules could be isolated. Therefore, describing the threshold K_{th} by more than one parameter, as Komber did in

[16] for different types of cast iron, is not necessary for nodular cast iron. The coefficient of determination illustrated in Figure 4 shows only a slight improvement compared to the fit using only the number of nodules per square millimeter. One can also see that the scatter of both empirical fits is very high, resulting in a quite low coefficient of determination. The fit parameters are summarized in Table 2.

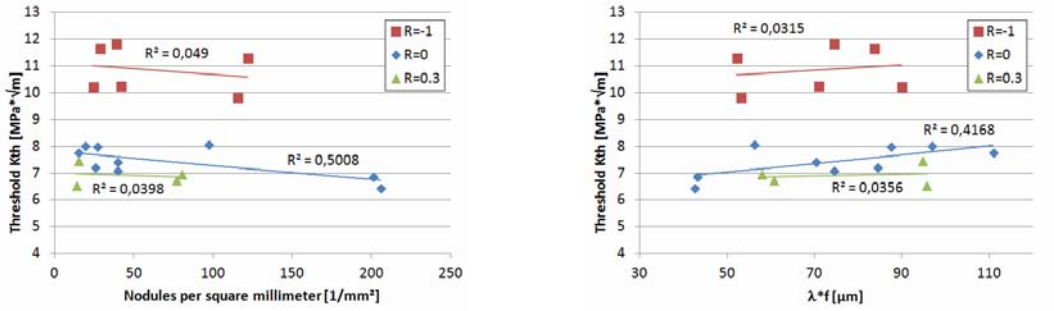

Figure 4: Threshold Kth in dependence of the number of particles per square millimeter (left) and the formalism used in [12,13] (right)

Table 2: Parameters of the empirical fit of the threshold K_{th}.

	Nodules/mm² [1/mm²]			λ*f [µm]		
	R=-1	**R=0**	**R=0.3**	**R=-1**	**R=0**	**R=0.3**
Slope	-0,0042	-0,0052	-0,0022	0,0097	0,0157	0,0037
y-intercept	11,11	7,82	7,01	10,16	6,27	6,63

Figure 5 shows a comparison of thresholds found in the literature [15,16,17]. As Zambrano already pointed out in [17], considerable differences are found in the resulting thresholds. The data presented in this paper shows good agreement with [15,16] for R=0 and R=0.3. Significant differences for the R=-1 tests have been found compared to [17]. It should be pointed out, that [15,16] used three-point bending specimen, [17] used edge cracked tension specimen and four point bending specimen have been used in the present investigations.

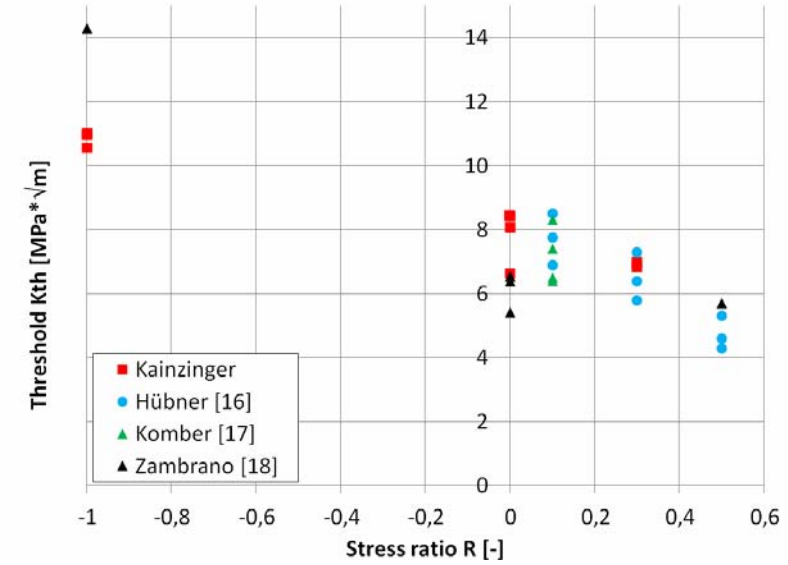

Figure 5: Comparison of thresholds found in the literature

4. Woehler Experiments

The Woehler experiments used for this paper have already been published in [6]. To improve the readability the results will be summarized shortly. For detailed information the reader is referred to the original paper.
Specimens have been taken from different sampling locations within the aforementioned wind turbine hub to cover a variety of different solidification conditions ranging from very slow solidification (coarse microstructure) in the center of a 100mm thick wall (position 1) to very fast solidification (fine microstructure) beneath chill irons (position 4). The results of these S/N curves are summarized in Figure 6. The fatigue strength increases with decreasing solidification time. In [6] an empirical model was proposed linking the parameters of the S/N curve with the local number of nodules per square millimeter. Good correlation was achieved between the model and the experiments. In the following part of this paper, a more physically based approach is proposed using the Kitagawa Takahashi diagram [4] modified by El Haddad [5].

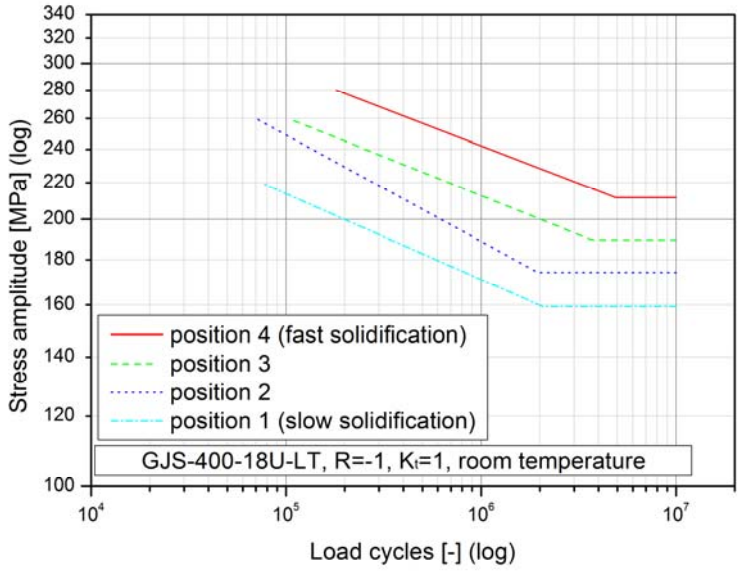

Figure 6: Results of the S/N curves from different sampling positions [8]

5. Fractographic Analysis

The fractured specimen surface has been analyzed using a scanning electron microscope. Micro-shrinkages have been found to be the dominant site of crack initiation (cf. Figure 7). This has also been confirmed by other authors, e.g. [18,19].

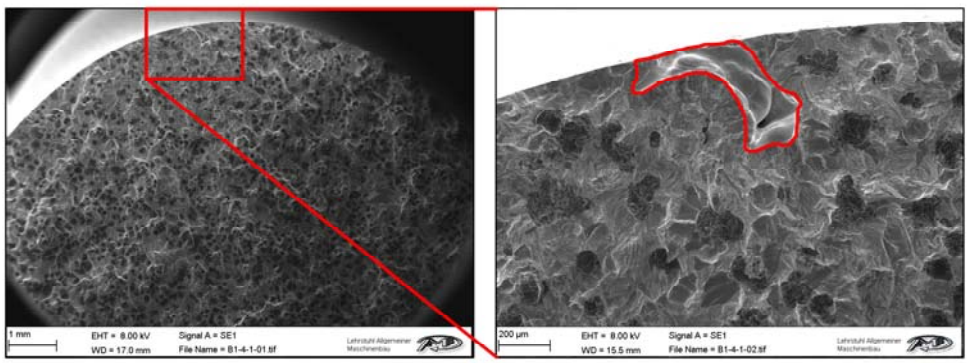

Figure 7: Micro-shinkages of different sizes found in the fractured specimen surface.

All micro-shrinkages were located at the specimen surface. Subsequent measurement of these micro-shrinkages has been carried out. The square root of the area [20] and the maximum dimension of the defects have been measured for all tested specimen. Some fracture surfaces revealed more than one micro-shrinkage, these specimens have not been evaluated due to the interaction effects of the micro-shrinkages.

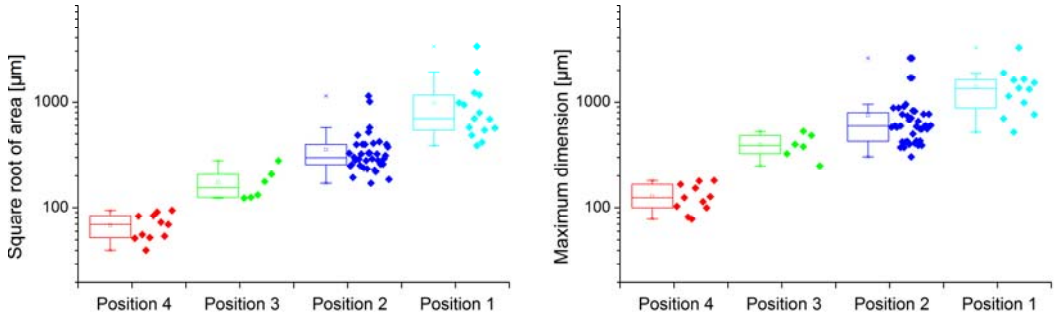

Figure 8: Box-plot of the size of the microshrinkages found in the fractured specimen surface. The square root of the area is displayed on the right side, the maximum dimenson on the left.

It has been observed that the size of the micro-shrinkages significantly decreases with decreasing solidification time (fine microstructure), which is illustrated by means of a box-plot in Figure 8. This trend is visible for both, the square root of the area as well as the maximum dimension.

6. Discussion

When considering both experimental results on their own, the observed trend is contradictory. The crack growth experiments indicate higher thresholds and lower crack growth rates (cf. [15]) for a coarse microstructure (slow solidification, respectively). This should result in better fatigue properties but the results of the fatigue tests show the exact opposite, a coarse microstructure leads to worse fatigue properties. The missing links are the micro-shrinkages of different sizes. Figure 8 shows the size of the shrinkages in dependence of the microstructure. Their mean values of the square root of their area ranges from 68µm for the fine microstructure up to 688µm for the coarse microstructure. This compensates the effect of the better crack growth properties of the coarse microstructure. The fatigue properties get worse, due to the disproportionally big size of the micro-shrinkages.

7. Local Fatigue Model

The Kitagawa Takahashi diagram modified by El Haddad, compensating the effects of short crack growth, will be used to describe the effect of micro-shrinkages on the fatigue behavior of ductile iron. The used equation is the following:

$$\sigma_a = \frac{\Delta K_{th}}{Y \cdot 2 \cdot \sqrt{\pi \cdot (a + a_0)}} \tag{1}$$

The threshold for crack propagation K_{th} is not constant throughout the material, it increases in case of a more coarse microstructure. For a better illustration of all sampling positions in a single diagram Eq. (1) has been normalized by being devided by the threshold:

$$\frac{\sigma_a \cdot 2}{\Delta K_{th}} = \frac{1}{Y \cdot \sqrt{\pi \cdot (a + a_0)}} \tag{2}$$

The corresponding threshold for the S/N curves from positions 1-4 have been calculated using the empirical fit using only the number of graphite nodules per square millimeter in Figure 4. A constant geometry factor of Y=0.65 has been used.
The El Haddad approach requires a fatigue limit of a defect free material to calculate the intrinsic crack length a_0. Since no defect free material was available for this research, the parameter a_0 was fitted to yield the best correlation between the estimated and the tested fatigue limits. A value of a_0=425µm led to the best results. This value of a_0 results in a theoretical fatigue limit of the defect free material of 212 to 231MPa, depending on the used threshold (10.1 and 11MPam^1/2, respectively). This defect free fatigue limit shows very good correlation with the empirical model proposed in [8].

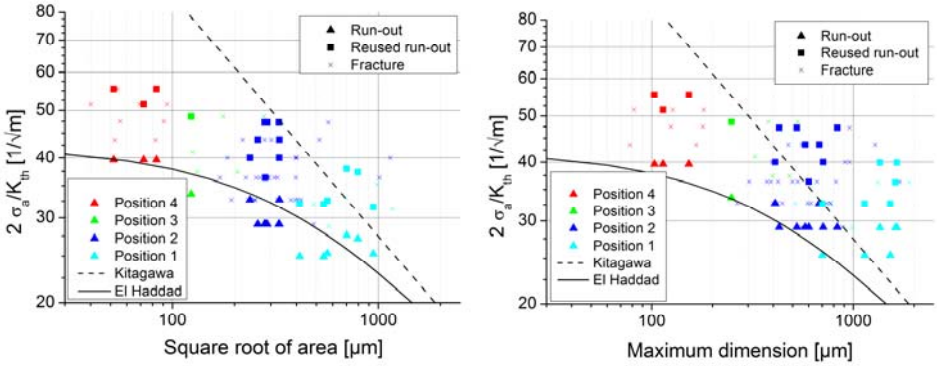

Figure 9: Normalized Kitagawa Takahashi diagram for all four sampling positions using the square root of the area (left) and the maximum dimension (right).

The Kitagawa Takahashi diagram using the square root of the area and the maximum dimension of the micro-shrinkage is illustrated in Figure 9. Using the square root of the area results in an overall good correlation, the use of the maximum dimension always led in conservative estimations of the fatigue limit. This is also emphasized in Figure 10, where the estimated fatigue limit is plotted against the experimental result. Therefore, the mean defect size (square root of area or maximum dimension, respectively) has been used to calculate the corresponding estimation using Eq. (1).

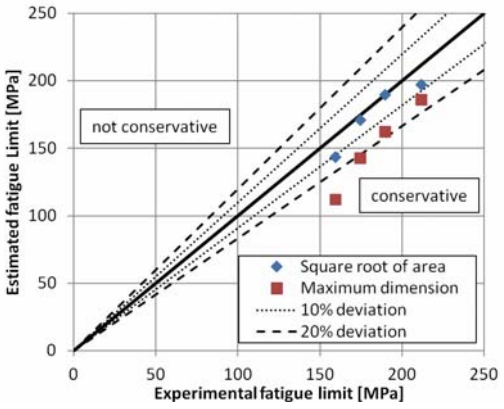

Figure 10: Comparison of the experimental and estimated fatigue limits.

8. Summary

- Fatigue crack growth as well as conventional fatigue tests have been carried out on specimens from different locations within a wind turbine hub. The sampling locations represent different solidification conditions which result in different microstructures.
- It has been found, that the fatigue crack propagation properties as well as the parameters of the S/N curve significantly depend on the local microstructure. The threshold for crack propagation K_{th} decreases with decreasing solidification time (fine microstructure), the fatigue properties increase with decreasing solidification time (resulting in a large number of particles per square millimeter).
- A contradictory trend has been found comparing the crack growth and conventional fatigue tests with different microstructures. Crack growth experiments show better fatigue properties for coarse microstructures, whereas conventional fatigue tests showed worse properties.
- Micro-shrinkages have been found to be the dominant site for crack initiation. The size of these micro-shrinkages compensates for the contradictory trend mentioned above.
- Subsequently, the local fatigue crack properties and the size of the micro-shrinkages are combined in the Kitagawa Takahashi diagram modified by El Haddad. Using the square root of the defect area leads to very good results. The maximum dimension always leads to conservative results.

Acknowledgements

Financial support by the Austrian Federal Government (in particular from the Bundesministerium fuer Verkehr, Innovation und Technologie and the Bundesministerium fuer Wirtschaft und Arbeit) and the Styrian Provincial Government, represented by Oesterreichische Forschungsfoerderungsgesellschaft mbH and by Steirische Wirtschaftsfoerderungsgesellschaft mbH, within the research activities of the K2 Competence Centre on ‘Integrated Research in Materials, Processing and Product Engineering’, operated by the Materials Center Leoben Forschung GmbH in the framework of the Austrian COMET Competence Centre Programme, is gratefully acknowledged. Furthermore, the authors would like to thank their project partners SHW Casting Technologies GmbH and AMSC Austria GmbH for their support.

References

[1] Rechnerischer Festigkeitsnachweis furr Maschinenbauteile, FKM Richtlinie, 4. Ausgabe, 2002.
[2] Guideline for the Certification of Wind Turbines, Germanischer Lloyd, Edition 2003 with Supplement 2004.
[3] J. Strum: Cast iron - a predictable material, World Foundry Congress, 2010.
[4] H. Kitagawa, S. Takahashi: Applicability of fracture mechanics to very small or cracks in the early stage, Proc. Of the second int. Conference on mech. behaviour of materials, ASM, 1976; 627-631.
[5] M.H. El Haddad, K.N. Smith, T.H. Topper: "Fatigue crack propagation of short cracks", ASME transactions, vol. 101, 1979.
[6] P. Kainzinger, C. Guster, M. Severing, A. Wolf: Abschaetzung der lokalen Woehlerlinie von Gusseisen mit Kugelgraphit aus der Giesssimulation, DVM-Bericht 139, 2012
[7] DIN EN 1563, Giessereiwesen - Gusseisen mit Kugelgraphit, 2011
[8] ASTM E647, Standard Test Method for Measurement of Fatigue Crack Growth Rates, 2010
[9] A. Leitgeb, Bruchmechanik und schadenstolerante Konstruktion im Automobilbau, PhD thesis, Montanuniversitaet Leoben, 2010.

[10] Standard Practice for Statistical Analysis of Linear or Linearized Stress-Life (S-N) and Strain-Life (e-N) Fatigue Data, ASTM E 739-91, 1998.
[11] E. Haibach, A Likely Explanation of Very High Cycle Fatigue in Steel, FEMFAT User Meeting, 2011.
[12] D. Degnel, Die arcsin $\sqrt{p}$ -Transformation - ein einfaches Verfahren zur grafischen und rechnerischen Auswertung geplanter Woehlerversuche, Journal of Materials Technology, 1975, Issue 8, P. 253-288.
[13] W. Weibull, Fatigue Testing and Analysis of Results, 1961.
[14] G. Blom, On linear estimates with nearly minimum variance, Ark. Mat. 3, P. 365-369, 1956.
[15] P. Huebner, H. Schlosser, G. Pusch, H. Biermann, Load history effects in ductile cast iron for wind turbine components, International Journal of Fatigue, 2007
[16] B. Komber Bruchmechanische Bewertung des Rissausbreitungsverhaltens ferritischer Gusseisenwerkstoffe bei zyklischer Beanspruchung, PhD thesis, TU Bergakademie Freiberg, 1995.
[17] H. R. Zambrano: Fracture toughness and growth of short and long fatigue cracks in ductile cast iron EN-GJS-400-18-LT, 2011
[18] M. Wohlfahrt: Einfluesse auf die Schwingfestigkeit von Gusseisen und deren Einbindung in die Berechnung der Bauteillebensdauer, VDI Report Nr. 2122, 2011.
[19] B. Pyttel, I. Brunner, D. Schwerdt, C. Berger: Influence of defects on fatigue strength and failure mechanisms in the VHCF-region for quenched and tempered steel and nodular cast iron, International Journal of Fatigue, 2012
[20] Y. Murakami: Metal fatigue: Effects of small defects and nonmetallic inclusions. Elesevier, 2002